



Embedded atom method potential for hydrogen on palladium surfaces

Ryan A. Ciuffo¹ · Graeme Henkelman¹

Received: 23 June 2020 / Accepted: 26 October 2020
© Springer-Verlag GmbH Germany, part of Springer Nature 2020

Abstract

The development of transferable interatomic potentials for the diffusion of hydrogen on palladium surfaces can be of significant value for performing molecular simulations. These molecular simulations can, in turn, lead to a better understanding of palladium-hydrogen interactions at the atomic scale. Here, we have built upon previous work to develop an analytical palladium-hydrogen-embedded atom method (EAM) potential to better describe the potential energy surface for hydrogen on palladium surfaces. This EAM potential reproduces minima and transition states calculated with density functional theory for hydrogen on Pd(111) and Pd(110) surfaces. Additionally, this potential was tested by simulating the long timescale dynamics of hydrogen adsorbed on Pd(111). Our simulations show a barrier of ca. 0.49 eV for hydrogen diffusion into the bulk of Pd(111), which is consistent with experimental results.

Keywords Embedded atom method · Palladium hydride · Hydrogen adsorption and diffusion · Adaptive kinetic Monte Carlo

Introduction

The palladium-hydrogen system has attracted attention from applications ranging from catalysis to hydrogen purification and storage [1–3]. Palladium-hydrogen adsorption and absorption have also been studied in detail in vacuum, which has provided a fundamental understanding of the formation of palladium hydrides [4–7]. However, due to the importance of the interactions of hydrogen with palladium, either on the surface or in the bulk, there has been a desire to model these interactions to garner a better atomistic understanding. An example, where such an understanding of the interaction of hydrogen with palladium, both on the surface and in the bulk, is of importance, is the reductive pretreatment of palladium catalysts. These pretreatments are typically derived empirically without a detailed scientific understanding of the atomistic processes that are occurring. However, since these pretreatment methods occur over long time scales (hours to days), modern *ab initio*-based computational methods are not capable of directly simulating the

processes. To overcome this issue, empirical potentials such as the embedded atom method (EAM) can be used to reduce computational costs while increasing the accessible simulation time [8–10]. By using an empirical potential to gain atomistic insight into the evolution of catalytic surfaces, we can move towards tailoring catalytic pretreatments.

For the palladium hydride system, a number of EAM potentials have been developed to study the low (α) and high (β) hydrogen content phases. Zhou et al. developed an EAM potential based on a polynomial fit to the tabulated Pd potential data proposed by Foiles et al., which was able to predict the α and β phase miscibility gap [11–13]. Park et al. then developed a Pd-H EAM potential which also used a power series to fit the tabular Pd potential data from Foiles et al. [14]. Later, Hijazi et al. produced an analytical EAM potential for the Pd-H system, which was able to predict a number of physical properties of bulk palladium hydrides [15]. Of these analytic potentials, however, there remains an inability to accurately describe adsorbed hydrogen on palladium surfaces. The ability to model hydrogen adsorption on Pd surfaces is necessary to model the effects that hydrogen exposure has on Pd catalysts, as adsorption and surface diffusion are precursors to diffusion into the bulk [16]. Here, we build upon the work by Hijazi et al. [15] and fit an analytic Pd-H EAM potential that can accurately describe the potential energy surface (PES) of hydrogen adsorbed on palladium surfaces.

✉ Graeme Henkelman
henkelman@utexas.edu

¹ Department of Chemistry and the Oden Institute for Computational Engineering and Science, University of Texas at Austin, Austin, TX 78712, USA

Embedded atom method

In the embedded atom method, the total energy of the system can be written as:

$$E_{tot} = \sum_{j=1}^N F_i(\rho_i) + \frac{1}{2} \sum_{i=1}^N \sum_{\substack{j=1 \\ j \neq i}}^N \varphi_{ij}(r_{ij}) \quad (1)$$

$$\rho_i = \sum_{\substack{j=1 \\ j \neq i}}^N f_j(r_{ij}) \quad (2)$$

where E_{tot} is the total internal energy, ρ_i is the electron density of atom i due to all other atoms, F_i is the energy to embed atom i into an electron density ρ_i , φ_{ij} is a two-body interaction potential between atoms i and j , r_{ij} is the distance between atoms i and j , and f_j is the electron density of atom j as a function of the distance from its center. To describe the Pd-Pd and H-H interactions, we have kept the analytical form proposed by Hijazi et al. [15] where the embedding function for Pd is taken as:

$$F_{Pd}(\rho) = F(\rho_e) \left[1 - \eta \ln \left(\frac{\rho}{\rho_e} \right) \right] \left(\frac{\rho}{\rho_e} \right)^n \quad (3)$$

and

$$\rho(r) = f_e e^{-\chi(r-r_e)} \quad (4)$$

where f_e is a scaling constant defined by the relationship $f_e = E_c/\Omega$ where E_c is the cohesive energy and Ω is the atomic volume, r_e is the equilibrium bond length, and χ is a fitting parameter. The two-body potential for Pd-Pd and H-H are defined as:

$$\varphi_{PdPd} = -\phi \left[1 + \delta \left(\frac{r}{r_e} - 1 \right) \right] e^{-\beta_{PdPd} \left(\frac{r}{r_e} - 1 \right)} \quad (5)$$

$$\varphi_{HH} = D_{HH} \left(\beta_{HH} e^{-\alpha_{HH}(r-r_{0,HH})} - \alpha_{HH} e^{\beta_{HH}(r-r_{0,HH})} \right) \quad (6)$$

where ϕ , δ , β_{PdPd} , D_{HH} , β_{HH} , and α_{HH} are all adjustable parameters. The embedding energy for hydrogen is expressed using the form presented by Hijazi et al. as:

$$F_H(\rho) = -c_H \left(\frac{1}{2+d_H} (\rho + \varepsilon_H)^{2+d_H} - \frac{a_H + b_H}{1+d_H} (\rho + \varepsilon_H)^{1+d_H} + \frac{a_H b_H}{d_H} (\rho + \varepsilon_H)^{d_H} \right) \quad (7)$$

and

$$\rho(r) = C_H e^{-\delta_H r} \quad (8)$$

where a_H , b_H , c_H and d_H are fitting parameters, C_H and δ_H are positive constants, and ε_H is a constant with the value 0.054. Lastly, the Pd-H pair potential is expressed using a Morse potential with the form

$$\varphi_{PdH} = D_{PdH} \left(1 - e^{-a_{PdH}(r_{ij}-r_{oPdH})} \right)^2 - D_{PdH} \quad (9)$$

where D_{PdH} , α_{PdH} , and r_{oPdH} are fitting parameters. Here, we keep the Pd-Pd and H-H terms proposed by Hijazi et al. (Eqs. 3–6, 8), and set out to fit new parameters for the Pd-H terms (Eqs. 7 and 9).

Fitting procedure

The parameters in Eqs. 7 and 9 were determined by minimizing the error in energies and geometries with respect to a set of 10 Pd-H configurations which were calculated with DFT (details in [Computational details](#) section). The structures used for fitting included atomic hydrogen adsorbed to an fcc surface site on Pd(111) (H_{fcc}), hydrogen in a Pd(111) subsurface octahedral site (H_{oct}), and hydrogen in a Pd(111) subsurface tetrahedral site (H_{tet}). In addition to these three local minima, the transition states between $H_{fcc} \rightarrow H_{oct}$, $H_{fcc} \rightarrow H_{hcp}$ on Pd(111) and the transition of hydrogen in bulk Pd from $H_{oct,b} \rightarrow H_{tet,b}$ (as opposed to the above mentioned subsurface H_{oct} and H_{tet} sites) were used to represent higher energy structures. To capture the local curvature of the H-Pd interaction, a set of structures were included where the z coordinate of hydrogen was fixed at 0.1 Å above and below the H_{fcc} minima on Pd(111). Additionally, the energy of images to the left and right of the $H_{fcc} \rightarrow H_{hcp}$ transition state was used to capture the curvature at higher energies and reduce the chance of fitting artificial minima at the transition states. From the above structures, we were able to capture local minima, local maxima, and local curvatures in our fitting procedure. A Monte Carlo algorithm, implemented in Python, was used to minimize the error between the binding energies and geometries for the above listed minima and the relative energies for the above listed transition and intermediate states.

Computational details

All EAM calculations were performed with the large-scale atomic/molecular massively parallel simulator (LAMMPS) [17]. All density functional theory (DFT) calculations were performed using the Vienna ab initio simulation package [18–21]. For DFT calculations, the projector-augmented wave framework was used to treat interactions between the core and valence electrons [22, 23]. Electronic exchange and correlation were described with the generalized gradient approximation—Perdew-Burke-Ernzhof functional [24, 25]. A cutoff energy of 400 eV was used for all calculations. Methfessel-Paxton smearing was employed with a width of 0.2 eV [26]. All of the training Pd-H slabs were modeled as 4×4 unit cells with four atomic layers where the bottom two layers were frozen in bulk positions. For the PES mapping calculations, a (2×2) unit cell with five atomic layers was used where the bottom two atomic layers were frozen to bulk positions.

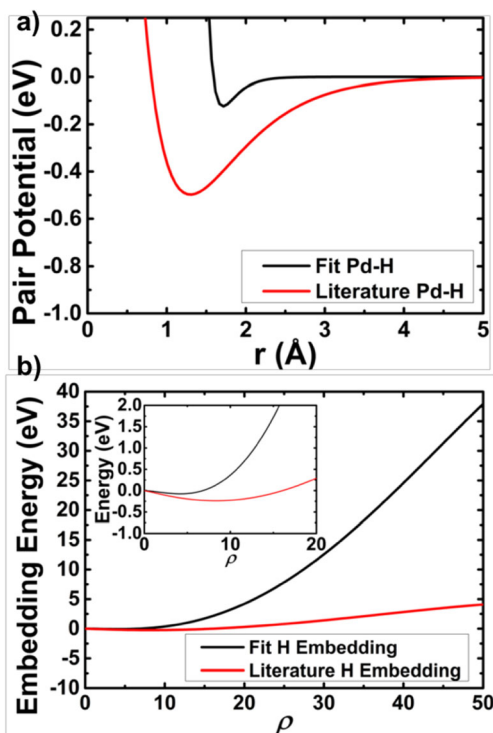


Fig. 1 Our fit and literature (a) Pd-H pair potential and (b) hydrogen embedding term. [15]

Periodic slabs were separated by 12 Å of vacuum. The bulk Pd-H calculations were performed with a 2x2x2 unit cell with periodic boundary conditions. For the DFT calculations, the Brillouin zone was sampled with a 2 × 2 × 1, a 5 × 5 × 1, and a 11 × 11 × 11 mesh using the Monkhorst-Pack k-points scheme for the training slabs, PES mapping slabs, and bulk calculations, respectively [27]. All calculations were allowed to relax until the forces on each atom were less than 0.05 eV/Å. An optimized lattice constant of 3.89 Å was used for the EAM calculations and 3.94 Å for the DFT calculations.

The adaptive kinetic Monte Carlo (aKMC) method as implemented in the EON package was used to simulate the dynamical evolution of hydrogen on Pd(111) [28–30]. The energy and force of the system were evaluated with our EAM potential. The system was modeled as a 4 × 4, six-layer slab with the two bottom-most layers frozen to bulk positions. The dimer method was used to explore possible reaction mechanisms and product states [31]. At each new state, dimer minimum-mode following searches were performed until a confidence value for the rate table of 0.95 was reached. The rate constant for each event was computed from the Arrhenius

equation $r = A \exp\left(\frac{-\Delta E}{k_b T}\right)$, where ΔE , T , and k_b are the energy barrier, temperature, and the Boltzmann constant, respectively. The pre-exponential factor was calculated explicitly from harmonic transition state theory where $A = \frac{\prod_i^{3N} \nu_i^{init}}{\prod_i^{3N-1} \nu_i^\ddagger}$, where ν_i^{init} and ν_i^\ddagger are the positive normal mode frequencies of the initial and saddle points, respectively. The absorbing Markov chains method was used to improve simulation efficiency by determining the escape time from superbasin states [32].

Results

The Pd-H pair potential and hydrogen embedding function are shown in Fig. 1. The corresponding parameters for the EAM potential (Eqs. 7 and 9) are listed in Table 1. As seen in Fig. 1a, there is a qualitative difference between the new Pd-H pair potential and the literature potential [15]. The binding energy of the fit is ca. −0.1 eV, whereas that from the literature [15] is ca. −0.45 eV. Additionally, the fit Pd-H pair potential has a longer equilibrium bond length of 1.71 Å as compared to the literature value of 1.30 Å [15]. This better matches the experimental equilibrium bond length of 1.55 Å for the Pd-H dimer in vacuum [33]. It also better matches our bond lengths calculated from DFT (Table 2). As shown in Fig. 1b, there is also a significant change in the hydrogen embedding term; a more positive slope is seen for the fit as compared to the literature [15]. In the low-density region (below $\rho = 7$) of the fit potential (Fig. 1b, inset), the embedding term is slightly negative, with an energy minimum of ca. −0.08 eV. Above $\rho = 7$, there is a significant repulsive potential energy gradient. The minimal contribution from the embedding term at low densities (which would be expected for adsorbed hydrogen) leads to a greater contribution to the total energy from the Pd-H pair potential. In contrast, the literature [15] embedding term results in a significant negative energy contribution at electron densities below $\rho = 17$ (with an energy minimum of −0.24 eV) and only a mild positive potential energy gradient at higher densities. This significant negative energy contribution at densities up to $\rho = 17$ helps explain the significant stabilization of bulk hydride formation seen in the literature EAM potential [15].

Table 2 shows the energy and geometry results from our EAM and DFT calculations for the structures used to fit our EAM potential. It is seen that there is good agreement between

Table 1 Fitting parameters for Eqs. 7 and 9 to describe the Pd-H interactions

D_{PdH}	α_{PdH}	r_{oPdH}	a_H	b_H	c_H	d_H
0.123452	5.583967	1.712318	4.245745	69.595833	0.000104	1.672605

Table 2 Energies and bond lengths for hydrogen on Pd(111) and bulk Pd

	E_{Hfcc} (eV)	E_{Hoct} (eV)	E_{Htetr} (eV)	r_{Hfcc} (Å)	r_{Hoct} (Å)	r_{Htetr} (Å)	$H_{\text{fcc}} \rightarrow H_{\text{oct}}$ TS (eV)	$H_{\text{oct,b}} \rightarrow H_{\text{tetr,b}}$ TS (eV)	$H_{\text{fcc}} \rightarrow H_{\text{hcp}}$ TS (eV)
DFT	0.63	0.29	0.28	1.81	1.77/2.42	1.68	0.35	0.25	0.16
EAM	0.57	0.34	0.34	1.76	1.74/2.32	1.73	0.27	0.23	0.06

Binding energies for DFT are relative to a clean Pd(111) slab and $\frac{1}{2}$ H₂. Binding energies for EAM are relative to a Pd(111) slab with hydrogen held at an infinite distance

the EAM- and DFT-binding energies, geometries, and transition state barriers. The EAM potential shows slight under-binding for surface hydrogen when compared to the DFT values. In contrast, there is a slight over-binding of subsurface hydrogen for the EAM potential when compared to DFT. Finally, the EAM- and DFT-calculated transition state barriers align well with each other. To ensure that our EAM potential can accurately describe regions of the PES that were not included in the training set, we mapped the PES for Pd(111) using both DFT and EAM. The results, seen in Fig. 2, are in good agreement with each other. For both, threefold hollow sites are seen to be the most stable, followed by bridge, and then top sites. Additionally, smooth transitions are seen between minima.

To test the transferability of the EAM potential, the PES of hydrogen on the Pd(110) surface was calculated with both DFT and EAM. As seen in Fig. 3, there is good agreement between the PES produced from DFT (Fig. 3a) and the PES produced from EAM (Fig. 3b). For the 110 surface, a slight

over-binding can be observed for surface hydrogen using the EAM potential. However, it should be noted that our EAM potential can accurately describe the pseudo-hollow site as the true minima, followed by the short bridge, and then the long bridge. This stands out, as EAM potentials for hydrogen on other metals, such as Cu, have been unable to accurately reproduce the PES of the (110) surface [34]. This finding shows the transferability of our EAM potential to structures outside of our training set.

Using our EAM potential, we performed long time scale simulations of hydrogen diffusion on Pd(111) using the adaptive kinetic Monte Carlo (aKMC) method [28, 29]. The diffusion of a single hydrogen adatom on a Pd(111) surface was modeled at 300 K. The absorbing Markov chains method was used to improve the efficiency of simulation by grouping fast transitions into superbasins via a transition counting scheme [30, 32]. With this method, the surface diffusion states of hydrogen were treated as a single superbasin, where

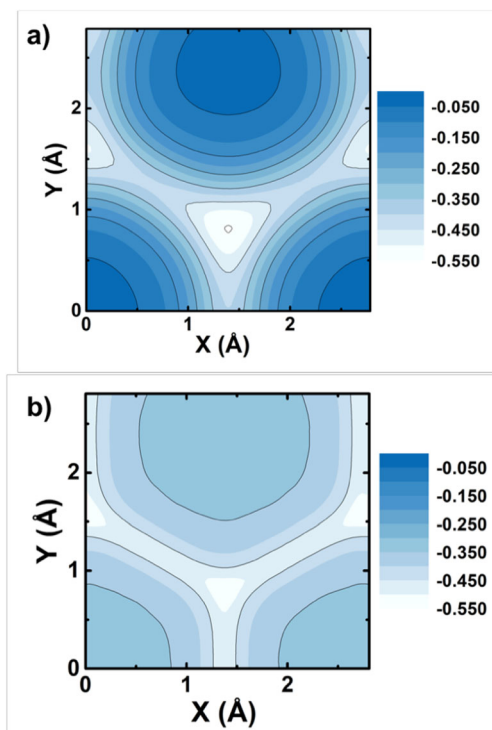


Fig. 2 Potential energy surfaces for hydrogen on Pd(111) calculated using (a) DFT and (b) our EAM potential. The energy shown is the binding energy (eV) for hydrogen on the surface at a coverage of $\theta = 0.25$

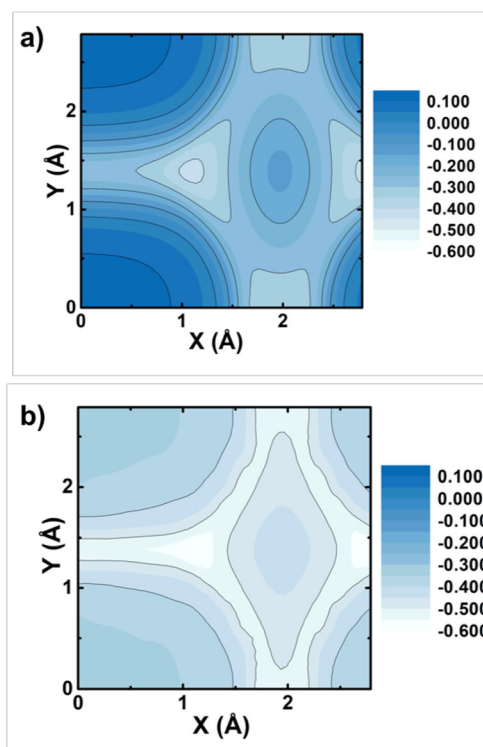
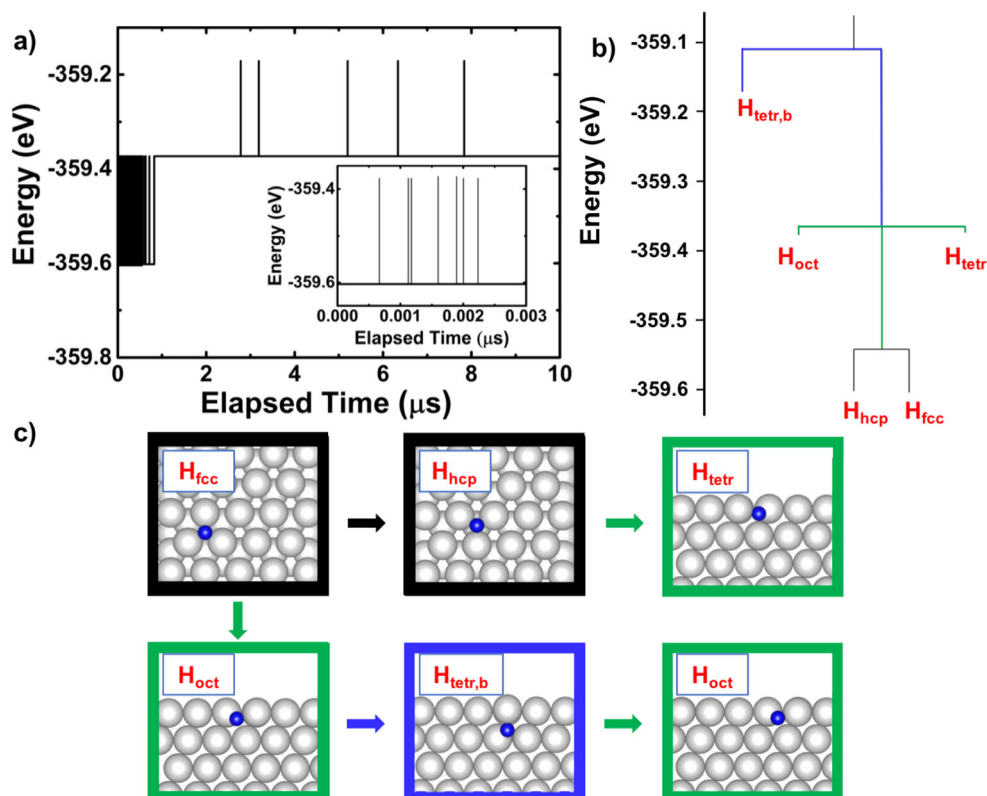


Fig. 3 Potential energy surface for hydrogen on Pd(110) calculated using (a) DFT and (b) our EAM potential. The energy shown is the binding energy (eV) for hydrogen on the surface at a coverage of $\theta = 0.25$

Fig. 4 **a** The time evolution of the total energy of hydrogen on Pd(111) at 300 K. Inset magnification of the first 0.003 μ s. **b** A disconnectivity graph from the 5 unique states visited in the aKMC simulation. Hydrogen states in the first subsurface are colored green. Hydrogen states in the second subsurface (bulk like sites) are colored blue. **c** Depictions of the states labeled in b and c where the white spheres are Pd and the blue spheres are H. The black, green, and blue outlines refer to the colors from Fig. 4b



individual transitions between the surface H states were lost, but the transition times out of the superbasin were preserved. The time evolution of the total energy of hydrogen on Pd(111) can be seen in Fig. 4. Before 2.8 μ s, hydrogen is seen to diffuse across the Pd(111) surface from H_{fcc} to H_{hcp} sites by way of bridge sites. There is also diffusion from H_{fcc} to subsurface H_{oct} sites as well as from H_{hcp} to H_{tetr} sites. However, before 2.8 μ s, no transitions are seen between subsurface sites or into the second subsurface layer—all subsurface hydrogen resurfaces. After 2.8 μ s, diffusion to the subsurface was observed, where hydrogen migrates between H_{oct} sites via tetrahedral sites in the second sublayer ($H_{tetr,b}$). These transitions are depicted in Fig. 4c.

To better represent the diffusion of hydrogen into the bulk, a disconnectivity graph was produced using the minima and transitions from the aKMC simulation (Fig. 4b) [35–38]. Briefly, the endpoint of each vertical line in the disconnectivity graph represents a minimum from the aKMC calculation. A vertex which connects any two minima indicates the energy of the saddle point that connects the corresponding minima. A discretization of 0.002 eV was used to distinguish between unique states. In Fig. 4b, the lower black portion of the graph corresponds to hydrogen diffusion on the Pd(111) surface. The middle green portion corresponds to hydrogen in the first subsurface layer, while the upper blue portion corresponds to hydrogen diffusion into the second (bulk-like) subsurface layer. From the disconnectivity graph,

we see that the energy barrier to diffuse from a surface adsorbed hydrogen to a hydrogen in the bulk is ca. 0.49 eV. These results are in agreement with past experimental findings that show that hydrogen penetration into the bulk of Pd foils is the rate limiting step for hydrogen absorption, with a barrier of ca. 0.3–0.4 eV [39, 40].

Conclusions

Using a set of three local minima, three transition states, and the local curvature around one minimum and one transition state, we were able to fit an analytic EAM potential to describe the PES of hydrogen on palladium surfaces. This EAM potential was able to accurately reproduce the PES for hydrogen on Pd(111) and Pd(110). On Pd(110), the potential was able to capture the pseudo-hollow site as the local minima. Using the EAM potential, long time scale dynamics were performed to model hydrogen on Pd(111) at 300 K. It was seen that for the first 2.8 μ s, surface diffusion was dominant. Only after 2.8 μ s was diffusion into the bulk observed, which is consistent with past experimental findings that showed the bottleneck to hydrogen absorption is diffusion from the surface into the bulk.

Funding National Science Foundation (US) (CHE-1764230) and Welch Foundation (F-1841).

References

- Povel R, Feucht K, Gelse W, Withalm G (1989) Hydrogen fuel for motorcars. *Interdiscip Sci Rev* 14(4):365–373
- Knapton AG (1977) Palladium alloys for hydrogen diffusion membranes. *Platin Met Rev* 21(2):44–50
- Adams BD, Chen A (2011) The role of palladium in a hydrogen economy. *Mater Today* 14(6):282–289
- Gdowski GE, Felter TE, Stullen RH (1987) Effect of surface temperature on the sorption of hydrogen by Pd(111). *Surf Sci* 181:147–155
- Okuyama H, Siga W, Takagi N, Nishijima M, Aruga T (1998) Path and mechanism of hydrogen absorption at Pd(100). *Surf Sci* 401(3):344–354
- Behm RJ, Penka V, Cattania M-G, Christmann K, Ertl G (1983) Evidence for “subsurface” hydrogen on Pd(110): an intermediate between chemisorbed and dissolved species. *J Chem Phys* 78(12):7486–7490
- Kay BD, Peden CHF, Goodman DW (1986) Kinetics of hydrogen absorption by Pd(110). *Phys Rev B* 34(2):817–822
- Daw MS, Baskes MI (1984) Embedded-atom method: derivation and application to impurities, surfaces, and other defects in metals. *Phys Rev B* 29(12):6443–6453
- Daw MS, Foiles SM, Baskes MI (1993) The embedded-atom method: a review of theory and applications. *Mater Sci Reports* 9(June 1992):251–310
- Senftle TP, Janik MJ, Van Duin ACT (2014) A ReaxFF investigation of hydride formation in palladium nanoclusters via Monte Carlo and molecular dynamics simulations. *J Phys Chem C* 118(9):4967–4981
- Zhou XW, Zimmerman JA, Wong BM, Hoyt JJ (2008) An embedded-atom method interatomic potential for Pd-H alloys. *J Mater Res* 23(3):704–718
- Foiles SM, Hoyt JJ (2001) Computer simulation of bubble growth in metals due to He. Sandia Report SAND2001-0661
- Zimmerman JA, Zhou XW, Griffin J, Wong BM, Hoyt JJ (2007) Development of an inter-atomic potential for the Pd-H binary system. Sandia Report SAND2007-WXYZ
- Park YH, Hijazi I (2017) Development of physics based analytical interatomic potential for palladium-hydride. *J Mol Model* 23(4):1–11
- Hijazi I, Zhang Y, Fuller R (2018) A simple embedded atom potential for Pd-H alloys. *Mol Simul* 44(17):1371–1379
- Lynch JF, Flanagan TB (1973) An investigation of the dynamic equilibrium between chemisorbed and absorbed hydrogen in the palladium/hydrogen system. *J Phys Chem* 77(22):2628–2634
- Plimpton S (1997) Short-range molecular dynamics. *J Comput Phys* 117(6):1–42
- Kresse G, Hafner J (1993) Ab initio molecular dynamics for liquid metals. *Phys Rev B* 47(1):558
- Kresse G, Hafner J (1994) Liquid-metal—amorphous-semiconductor ab initio molecular-dynamics simulations of the liquid-metal-amorphous-semiconductor transition in germanium. *Phys Rev B* 49(20):14251
- Kresse G, Furthmüller J (1996) Efficiency of Ab-initio total energy calculations for metals and semiconductors using a plane-wave basis set. *J Am Water Works Assoc* 6:15–50
- Kresse G, Furthmüller J, Li YJ, Chen YJ, Walmsley JC, Mathisen RH, Dumoulin S, Roven HJ, Yip S, Supervisor T et al (1996) Efficient iterative schemes for ab initio total-energy calculations using a plane-wave basis set. *Phys Rev B* 54(16):11169–11186
- Kresse G, Joubert D (1999) Kresse, Joubert - unknown - from ultrasoft pseudopotentials to the projector augmented-wave method. *Phys Rev B* 59(3):11–19
- Bloch PE (1994) Projector augmented-wave method. *Phys Rev B* 50(24):17953–17979
- Perdew JP, Burke K, Ernzerhof M (1996) Generalized gradient approximation made simple - the PBE functional. *Phys Rev Lett* 77(18):3865–3868
- Perdew JP, Burke K, Ernzerhof M (1997) Generalized gradient approximation made simple. *Phys Rev Lett* 78:1396
- Methfessel M, Paxton AT (1989) High-precision sampling for Brillouin-zone integration in metals. *Phys Rev B* 40(6):3616–3621
- Monkhorst HJ, Pack JD (1976) Special points for Brillouin-zone integrations. *Phys Rev B* 13(12):5188–5192
- Xu L, Henkelman G (2008) Adaptive kinetic Monte Carlo for first-principles accelerated dynamics. *J Chem Phys* 129(11)
- Henkelman G, Jónsson H (2001) Long time scale kinetic Monte Carlo simulations without lattice approximation and predefined event table. *J Chem Phys* 115(21):9657–9666
- Chill ST, Welborn M, Terrell R, Zhang L, Berthet JC, Pedersen A, Jónsson H, Henkelman G (2014) EON: Software for long time simulations of atomic scale systems. *Model Simul Mater Sci Eng* 22(5)
- Henkelman G, Jónsson H (1999) A dimer method for finding saddle points on high dimensional potential surfaces using only first derivatives. *J Chem Phys* 111(15):7010–7022
- Novotny MA (1995) Monte Carlo algorithms with absorbing Markov chains: fast local algorithms for slow dynamics. *Phys Rev Lett* 74(1):1–5
- Lischka M, Groß A (2003) Hydrogen on palladium: a model system for the interaction of atoms and molecules with metal surfaces. *Recent Dev Vac Sci Technol* 661(2):111–132
- Bae CS, Freeman DL, Doll JD, Kresse G, Hafner J (2000) Energetics of hydrogen chemisorbed on Cu(110): a first principles calculations study. *J Chem Phys* 113(16):6926–6932
- Doye JPK, Miller MA, Wales DJ (1999) Evolution of the potential energy surface with size for Lennard-Jones clusters. *J Chem Phys* 111(18):8417–8428
- Evans DA, Wales DJ (2003) Free energy landscapes of model peptides and proteins. *J Chem Phys* 118(8):3891–3897
- Wales DJ, Miller MA, Walsh TR (1998) Archetypal energy landscapes. *Nature* 394(6695):758–760
- Becker OM, Karplus M (1997) The topology of multidimensional potential energy surfaces: theory and application to peptide structure and kinetics. *J Chem Phys* 106(4):1495–1517
- Namba K, Ogura S, Ohno S, Di W, Kato K, Wilde M, Pletikoscic I, Pervan P, Milun M, Fukutani K (2018) Acceleration of hydrogen absorption by palladium through surface alloying with gold. *Proc Natl Acad Sci U S A* 115(31):7896–7900
- Auer W, Grabke HJ (1974) The kinetics of hydrogen absorption in palladium (α - and β -phase) and palladium-silver-alloys. *Ber Bunsenges Phys Chem* 78(1):58–67

Publisher's note Springer Nature remains neutral with regard to jurisdictional claims in published maps and institutional affiliations.